Optical Diode Made from a Moving Photonic Crystal

Da-Wei Wang,[1,3] Hai-Tao Zhou,[2] Miao-Jun Guo,[2] Jun-Xiang Zhang,[2,*] Jörg Evers,[1,4] and Shi-Yao Zhu[1,2,3]

[1]*Beijing Computational Science Research Centre, Beijing 100084, China*

[2]*The State Key Laboratory of Quantum Optics and Quantum Optics Devices, Institute of Opto-Electronics, Shanxi University, Taiyuan 030006, China*

[3]*Centre of Optics Sciences and Department of Physics, The Chinese University of Hong Kong, Hong Kong, China*

[4]*Max-Planck-Institut für Kernphysik, Saupfercheckweg 1, 69117 Heidelberg, Germany*

(Received 3 September 2012; revised manuscript received 18 November 2012; published 25 February 2013)

Optical diodes controlling the flow of light are of principal significance for optical information processing. They transmit light from an input to an output, but not in the reverse direction. This breaking of time reversal symmetry is conventionally achieved via Faraday or nonlinear effects. For applications in a quantum network, features such as the abilities of all-optical control, on-chip integration, and single-photon operation are important. Here we propose an all-optical optical diode which requires neither magnetic fields nor strong input fields. It is based on a ''moving'' photonic crystal generated in a three-level electromagnetically induced transparency medium in which the refractive index of a weak probe is modulated by the moving periodic intensity of a strong standing coupling field with two detuned counterpropagating components. Because of the Doppler effect, the frequency range of the crystal's band gap for the probe copropagating with the moving crystal is shifted from that for the counter-propagating probe. This mechanism is experimentally demonstrated in a room temperature Cs vapor cell.

DOI: 10.1103/PhysRevLett.110.093901 PACS numbers: 42.70.Qs, 42.50.Gy

Optical diodes, also known as optical isolators [1], are used to isolate lasers from reflections in the actual devices to improve their stability. The class of media suitable for diode operation is constrained by the Lorentz reciprocal theorem, which states that, in linear and nonmagnetic media, the source and detection position for monochromatic light with certain polarization can be interchanged without modifying the transmission properties [2]. The magnetic Faraday effect, which breaks the time-reversal symmetry of a polarization rotation [1], and nonsymmetrically acting nonlinearities [3–7] can circumvent this constraint by violating its requirements. However, Faraday rotators are usually large and require magnetic fields, while nonlinearities require strong electric fields of the probe light. Attracted by potential applications in quantum networks of light, many new designs have been proposed enabling desirable features such as the ability to integrate the diode on a chip [8–13], to make it optically controllable [8,14,15], and to reduce its operation range to low field intensities even to the single-photon level [16]. An even more desirable prospect is the integration of the diode with optical information processing (such as storage and retrieving) components. In this way, convenient all-optical control becomes possible, and no additional optical isolation devices are needed. Proposals for optical isolation with this feature have not been raised up to now.

An important candidate for quantum optical information processing is the electromagnetically induced transparency (EIT) medium [17,18], which is optically controllable, and has been integrated on chips [19] and reduced to the single photon level [20]. An optical diode based on EIT not only inherits these features, but also could integrate the optical isolation function into the quantum information processing components. Recently, a nonmagnetic optical diode based on dynamic refractive-index modulation was proposed in an electro-optic metal-oxide semiconductor [13] and realized in opto-acoustic fibers [8] and on a silicon chip [21]. Here, we theoretically and experimentally demonstrate that the general principle of refractive index modulation enables diode operation with a very different, but much simpler, picture of a ''moving'' photonic crystal in an EIT system, which not only opens perspectives for all-optical optical diodes operating at low light intensities, but also enables novel photonic devices such as optically tunable mirrors and cavities.

The key element of the optical diode implementation proposed here is a photonic crystal generated from a periodic modulation of the optical properties of a medium, which leads to the formation of a band gap. Light is transmitted through the crystal if its frequency is outside the gap, but it is not transmitted if the frequency is inside the gap. A static photonic crystal has the same transmission properties for light of equal frequency incident from opposite directions. However, if the photonic crystal moves, due to the Doppler effect, the counterpropagating light is blueshifted and the copropagating light is redshifted in the reference frame of the moving photonic crystal [22]. If one of the shifted frequencies is inside the gap and the other is outside the gap, the optical diode is formed.

However, this naive picture raises the question of how the moving photonic crystal could be realized in practice. In the following, we will show how this is possible without

actually moving any material parts of the setup. Instead of using a conventional photonic crystal based on a periodic sequence of different materials, we use an optically controllable photonic crystal based on an EIT medium driven by a standing wave control laser field [23–26]. The standing wave pattern formed by two counterpropagating coupling fields imposes a periodic modulation on the refractive index of the EIT medium, which acts as a photonic crystal for a weak probe field. By detuning the two counterpropagating components of the standing wave slightly, the envelope of the standing wave and thus the optically induced photonic crystal can be rendered moving in the static EIT medium. It is, therefore, the standing wave pattern that moves rather than the medium itself.

Consider a three-level EIT system as shown in Fig. 1(a). The frequency difference between states $|i\rangle$ and $|j\rangle$ ($i, j = a, b, c$) is $\omega_{ij} \equiv \omega_i - \omega_j$, and the transition between $|a\rangle$ and $|c\rangle$ is forbidden by symmetry. The states $|a\rangle$ and $|b\rangle$ are coupled by a detuned standing wave $\mathbf{E}_c(t) = \hat{y}[E_1 \cos(\omega_1 t - k_1 x) + E_2 \cos(\omega_2 t + k_2 x)]$, where E_1 and E_2 are the amplitudes of the two counterpropagating fields with frequency ω_1 and ω_2 and relative detuning $\delta = \omega_2 - \omega_1$. The magnitudes of the wave vectors of field E_i are $k_i = \omega_i/c$. It is well known that the refractive index of the EIT medium is periodically modulated by the standing wave such that a photonic crystal is formed [23,24,26]. For $\delta = 0$, we have a static photonic crystal, and for $\delta \neq 0$ we have a moving photonic crystal with the velocity of the moving standing wave envelope

$$v = -\frac{\delta}{2\omega_c} c, \tag{1}$$

where $\omega_c = (\omega_1 + \omega_2)/2$. For $\delta \neq 0$, a sign reversal of the detuning $\delta \to -\delta$ changes the sign of the velocity, $v \to -v$, and the envelope moves in the opposite direction. Equation (1) is the origin of the time-reversal symmetry breaking required for the diode operation [27]. As δ and t only enter the analysis as a product, a time reversal $t \to -t$ can equivalently be regarded as a detuning reversal $\delta \to -\delta$ and thus a velocity reversal. Because of the Doppler shift, the transmission spectra of moving photonic crystals with velocity v and $-v$ ($v \neq 0$) will be shifted with respect to each other and thus the time reversal symmetry is broken.

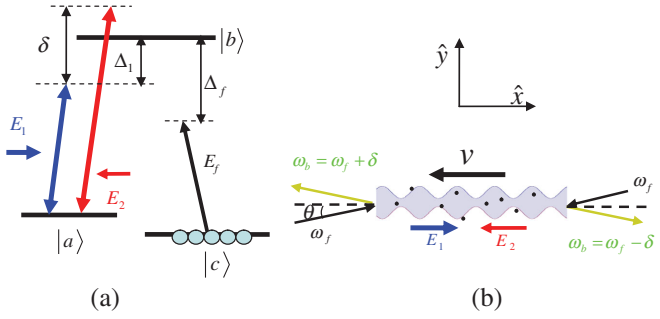

FIG. 1 (color). Implementation of the flying photonic crystal diode. (a) Level structure of the EIT medium. The coupling transition of the Λ-type three-level system is driven by a standing wave field with detuning δ between the two components. (b) The photonic crystal is formed by the standing wave pattern which flies to the left if $\delta > 0$. The black dots indicate the medium atoms with level structure as in (a). The photonic band gaps for probe light incident parallel or antiparallel to the crystal movement are shifted with respect to each other in frequency due to the Doppler effect and an optical diode is achieved.

A weak forward probe field $\mathbf{E}_f(t) = \hat{z} E_f \cos(\omega_f t - k_f x)$ probing the transition between $|c\rangle$ and $|b\rangle$ can be reflected by the moving photonic crystal. The band gap is formed at small detuning thanks to the large anomalous dispersion of the EIT medium in the transparency window [28]. Because of the Doppler effect, the reflected field $\mathbf{E}_b(t) = \hat{z} E_b \cos(\omega_b t + k_b x)$ has frequency $\omega_b = \omega_f + \delta$, while the frequency of the transmitted field remains the same. This important property was also verified experimentally with the setup described below and a frequency beating method. In the experiment, no beating signal between the incident and the transmitted field were observed. The probe and reflected fields in a static photonic crystal are usually treated by the transfer matrix [23] or, equivalently, the multiwave mixing method. For a moving photonic crystal, the latter is more convenient. The coupled-wave equations for probe and reflected fields are [24,26,29],

$$\frac{\partial}{\partial x} E_f(x) = -\beta_{12}(\omega_f) E_f(x) + i\kappa_{21}(\omega_b) e^{-i\Delta k_x x} E_b(x), \tag{2}$$

$$-\frac{\partial}{\partial x} E_b(x) = -\beta_{21}(\omega_b) E_b(x) + i\kappa_{12}(\omega_f) e^{i\Delta k_x x} E_f(x), \tag{3}$$

where $\beta_{ij}(\omega)$ ($\kappa_{ij}(\omega)$) are the attenuation (wave-mixing) coefficients for the probe field of frequency ω propagating along with the coupling field E_i and antiparallel to E_j. The coefficients are related to the linear and nonlinear medium susceptibilities χ_{ij}^L and χ_{ij}^{NL} by $\beta_{ij} = k_f \cos^{-1}\theta \mathrm{Im}\chi_{ij}^L/2$ and $\kappa_{ij} = k_f \cos^{-1}\theta E_1 E_2 \chi_{ij}^{\mathrm{NL}}/2$, where θ is the angle between the probe and the coupling fields, as shown in Fig. 1(b). $\Delta k_x = k_f \cos\theta[2 + (\mathrm{Re}\chi_{12}^L + \mathrm{Re}\chi_{21}^L)/2] - 2k_c$ is the wave vector mismatch along the $\hat{x}$ direction. In calculating χ_{ij}^L and χ_{ij}^{NL}, we take into account all orders of the coupling fields, E_1 and E_2, for the generation of the reflected field frequency, e.g., via four-wave ($\omega_b = \omega_f - \omega_1 + \omega_2$), six-wave ($\omega_b = \omega_f - \omega_1 + \omega_2 - \omega_1 + \omega_1$), and higher-order mixing. The summation of all orders of the coupling fields converges and can be performed by the technique of continued fractions [28,29]. The transmitted light does not acquire frequency shifts because it experiences only wave-mixing processes that lead back to the same frequency ω_f. For a sample of length L, the reflectance and transmittance are obtained as

$$R \equiv \left|\frac{E_b(0)}{E_f(0)}\right|^2 = \left|\frac{1}{\kappa_{21}(\omega_b)}\frac{e^{-(\lambda_+-\lambda_-)L}-1}{e^{-(\lambda_+-\lambda_-)L}[\lambda_+ + \beta_{12}(\omega_f)]^{-1} - [\lambda_- + \beta_{12}(\omega_f)]^{-1}}\right|^2, \quad (4)$$

$$T \equiv \left|\frac{E_f(L)}{E_f(0)}\right|^2 = \left|\frac{e^{(\lambda_++\lambda_-)L}(\lambda_- - \lambda_+)}{[\lambda_- + \beta_{12}(\omega_f)]e^{\lambda_- L} - [\lambda_+ + \beta_{12}(\omega_f)]e^{\lambda_+ L}}\right|^2, \quad (5)$$

where

$$\lambda_\pm = \frac{-i\Delta k_x - \beta_{12}(\omega_f) + \beta_{21}(\omega_b)}{2} \pm \frac{\sqrt{[i\Delta k_x - \beta_{12}(\omega_f) - \beta_{21}(\omega_b)]^2 + 4\kappa_{12}(\omega_f)\kappa_{21}(\omega_b)}}{2}. \quad (6)$$

The nonreciprocity from the perspective of wave mixing lies in the frequencies of the two coupled fields E_f and E_b in Eqs. (2) and (3). As shown in Fig. 1(b), for a forward (x direction) incident probe, the two coupled fields have frequencies ω_f and $\omega_b = \omega_f + \delta$, while for a backward ($-x$ direction) incident probe, the two coupled fields have frequencies ω_f and $\omega_b = \omega_f - \delta$. As both $\beta_{ij}(\omega)$ and $\kappa_{ij}(\omega)$ are frequency dependent, the reflectance and transmittance are different for the forward and backward probes, respectively.

In Figs. 2(a) and 2(b), the reflectance and transmittance R_L and T_L (R_R and T_R) for the left (right) probe are plotted as functions of the probe detuning $\Delta_f \equiv \omega_{bc} - \omega_f$. Here, the left (right) probe is along the direction of E_1 (E_2), as shown in Fig. 1(b). For the following experimental consideration, we use the parameters for three states of the caesium D_1 line, $6^2S_{1/2}$, $F = 4$ ($|a\rangle$), $6^2P_{1/2}$, $F = 4$ ($|b\rangle$), and $6^2S_{1/2}$, $F = 3$ ($|c\rangle$). We fix the one-photon detuning of the coupling field E_1 to $\Delta_{c1} \equiv \omega_{ba} - \omega_1 = 0$ and tune ω_2 such that $\delta = \pm 0.2\gamma_{bc}$, where γ_{bc} is the decoherence rate between levels $|b\rangle$ and $|c\rangle$. To characterize the diode performance of the optical diode, we use the contrast of the two transmittances $\eta = (T_L - T_R)/(T_L + T_R)$ in Fig. 2(c) for Figs. 2(a) and 2(b). For $\eta = 1$ ($\eta = -1$), a diode transmitting only the forward (backward) probe is achieved. From Fig. 2(a), we find two working regions for the optical diode with opposite probe directions and different probe frequencies. Around $\Delta_f = -0.1\gamma_{bc}$ (or $\Delta_f = 0.1\gamma_{bc}$), an optical diode is obtained that only allows transmission for the forward (backward) probe. As shown in Fig. 2(b), by changing the sign of δ (reversing the moving direction of the standing wave), the two working regions interchange their relative positions. As expected from the Doppler effect, the band gaps experienced by the forward and backward probes are shifted by δ with respect to each other.

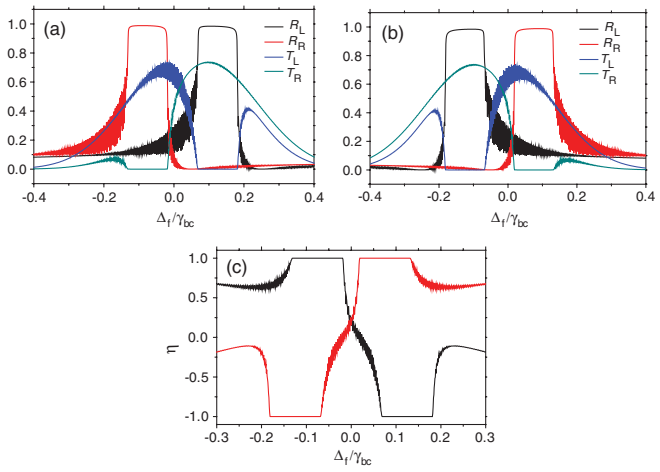

FIG. 2 (color). Reflection and transmission characteristics of the diode. The reflectances R_L (black) and R_R (red) and transmittances T_L (blue) and T_R (green) of the optical diode for both left (subscript 'L') and right (subscript 'R') incident light. The standing wave detuning is (a) $\delta = 0.2\gamma_{bc}$, and (b) $\delta = -0.2\gamma_{bc}$. The detuning of E_1 is zero, $\omega_1 = \omega_{ba}$. In (c), the contrast of the transmittance η for (a) (black) and (b) (red) is plotted. The Rabi frequency of the coupling field E_1 is $10\gamma_{bc}$ and $(E_2/E_1)^2 = 0.2$. The scalable product of the atomic density and the sample length is $NL = 3.5 \times 10^{13}$ cm^{-2} ($N = 3.5 \times 10^{14}$ cm^{-3}, $L = 1$ mm). The incident angle is $\theta = 0$. The dephasing rate between the two ground states is chosen as zero.

Figure 3 shows the transmission spectra of the probes in the two opposite directions as a function of δ. The purple areas (labeled as BG) between the two transmission branches are the band gaps. It can be seen that the pass bands of the forward probe correspond to band gaps of the backward probe, and vice versa over a range of δ. We also note that our moving crystal has properties different from those of a truly moving material photonic crystal. First, the band gap width increases linearly with the detuning δ, while for the "real" photonic crystal, the motion does not change the band gap width. Another difference to a real moving photonic crystal is that due to the inversion symmetry breaking by $E_1 \neq E_2$, the profiles of the two transmission spectra cannot be overlapped by a simple displacement of δ.

At fixed δ, only the two-photon detuning $\Delta_f - \Delta_{c1}$ is relevant in the spectra whose profile is not sensitive to the one-photon detuning of the coupling field $\Delta_{c1} \equiv \omega_{ba} - \omega_1$ as long as Δ_{c1} is not much larger than the Rabi frequency of the coupling fields (a few times larger is still fine). We can, therefore, tune the working point of the diode easily by changing Δ_{c1} while keeping δ fixed. This property also implies that the implementation is robust to thermal motion, for which the atom velocities only change the one-photon detunings but does not affect

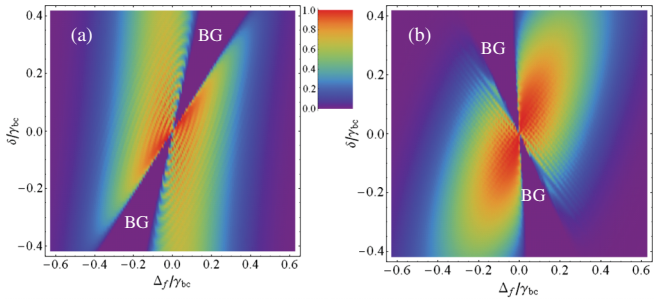

FIG. 3 (color). Band gap structure as a function of the detunings. The transmission spectra T_L in (a) and T_R in (b) are plotted as a function of the detuning δ. BG denotes the band gaps. The band gaps in (a) overlap the pass bands in (b) and vice versa. The parameters are the same as in Fig. 2.

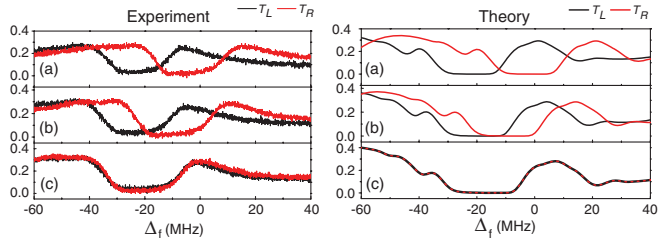

FIG. 4 (color). Experimental implementation of the diode in a thermal atom vapor. The figure shows the optical diode performance in a thermal atomic gas at temperature 28.6°C with 40 μW probe power and 50 mW coupling power. In the theoretical fitting, the Rabi frequency of the coupling fields ($E_1 = E_2$) is $2\pi \times$ 50 MHz, with $\gamma_{bc} = 2\pi \times 2.4$ MHz, cell length $L = 5$ cm, the atom density $N = 3.5 \times 10^{10}$ cm^{-3}, and the angle between coupling and probe fields $\theta = 0$. The detuning of E_1 is $\Delta_{c1} = -30$ MHz, and $\delta = -20$ MHz (a), -10 MHz (b), 0 MHz (c).

the two-photon detunings if the probe and coupling fields copropagate.

To demonstrate the principle of the above theoretical discussion based on the moving photonic crystal, we perform an experiment in a Cs vapor cell at room temperature, as described in Fig. 1. The powers of the two counterpropagating coupling fields in $\pm x$ directions are both 50 mW with e^{-2} full width 0.83 mm, and the probe power is 40 μW with width 0.50 mm. In order to improve the beam quality, the probe, coupling, and optical pumping beams pass through a single-mode fiber before the interaction with the atoms. The polarizations of the probe and coupling fields are orthogonal to each other and they have a frequency difference of about 9.2 GHz. Therefore, the coupling field can be easily filtered in optical communications. In the experiment, we use a 5 cm long cell at $T = 28.6°$C, such that the effective atom density is $N \approx 3.5 \times 10^{10}$ cm^{-3}. Note that while the strong absorption at room temperature greatly reduces the reflectance, it at the same time also reduces the transmission in the unwanted direction [28,29]. Therefore, high diode contrast can be achieved for reflectances significantly less than 100%. In Fig. 4, we plot the two transmissions for the probe in forward (black color) and backward (red color) directions, where the curves in left and the right columns are for experimental results and theoretical calculation, respectively. Because of the thermal atomic motion, the coefficients in Eqs. (2) and (3) are Doppler broadened, which we model by integrating over Maxwell's velocity distribution in the theoretical calculation. In Figs. 4(a)–4(c), we see that the gap separation between the forward and backward probes is equal to the control field frequency difference. The optical diode effect gradually disappears as the frequency difference approaches zero, which experimentally proves the principle of the optical diode based on the moving photonic crystal.

Although the FWHM of the Doppler broadening of the atoms is 360 MHz while the frequency difference between the two coupling fields is only 20 MHz, the nonreciprocity is very robust against the thermal fluctuations. Just like electrons in a metal, where a small drift velocity due to the applied electric field on the base of the large random electron velocity forms a current, the nonreciprocity comes from the unidirectional velocity of the detuned standing wave modulation in a medium gas with large but symmetrically distributed thermal velocities.

Theoretical calculation and experiments show that the gap appears near the two-photon resonance, $\Delta_f = \Delta_{c1}$ (Δ_{c2}) [17]. Therefore, the gap position and thus the working region of the optical diode can be tuned by varying the central frequency of the two coupling fields and their difference.

The probe power, which is 40 μW in Fig. 4, can be reduced to 10 μW without significant degradation of the diode performance. But when the probe field becomes too weak (below 5 μW in our experiment), the transmission is dominated by noise from the thermal fluctuations at room temperature [30]. Fortunately, the quantized energy level structure in atoms provides several routes to improve the performance of the optical diode. To reduce the absorption for weak field, we can introduce an additional 852 nm pumping field between $|c\rangle$ and a fourth level $|6^2P_{3/2}, F=4\rangle$. Then, saturation together with the V-type EIT effect greatly reduces the absorption. In Fig. 5, we plot the transmission spectra for the forward and backward probe fields with the additional 1 mW pumping field (e^{-2} full width 0.8 mm). The transmission reaches about 60% with a low probe power of 5 μW. Good diode performance can still be achieved with probe powers below 1 μW. However, to operate the optical diode at extremely low light intensities, it needs to be cooled down to very low temperatures to reduce the absorption from thermal noise.

EIT is a hallmark effect of quantum optics, well studied both in theory and in experiments [18], and has been integrated on chips [19,31] and reduced to the single photon level [17,20]. This, together with the flexible and robust scaling of our method to different parameter regimes, opens perspectives for optical diodes operating at low light levels across a broad range of media; e.g.,

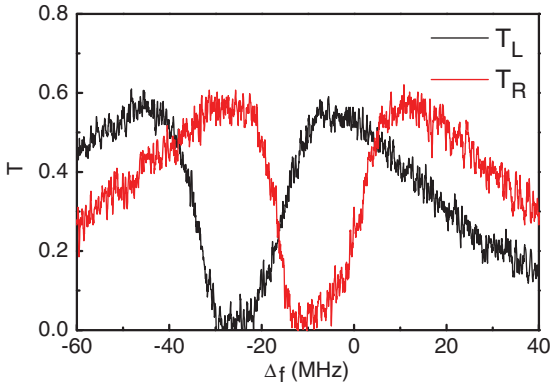

FIG. 5 (color). The transmission spectra with an additional 1 mW, 852 nm pumping field coupling $|c\rangle$ and $|6^2P_{3/2}, F=4\rangle$. The power of the probe field is 5 μW. All other parameters are the same as in Fig. 4(a).

integrated in small solid state devices. Our optical diode can be implemented in the same light information control system with EIT [19,24] by introducing another lower level to the original lambda system. This would lead to two lambda systems, one for controlling the bit and the other for optical isolation.

Going beyond the concept of a diode, a moving photonic crystal with high reflectance as in Fig. 2 can also be exploited to construct novel photonic devices. For example, the moving crystals can serve as the walls of a cavity which allow photons to enter but prevents them from leaving, or vice versa. The properties of this cavity can dynamically be controlled via the ''velocities'' of the walls, e.g., to trap or release photons on demand. Furthermore, the probe photon frequency can be modulated by dynamically changing the velocities of the walls, due to the velocity-dependent reflectivity (and reflection frequency).

In conclusion, we proposed and experimentally implemented an optical diode based on a moving photonic crystal, which is generated by a moving standing wave due to different frequencies for the two propagating fields in an EIT medium. The moving crystal is optically induced without actually moving any material parts. The diode is controlled by optical fields independent of the signal field, and can be implemented in a broad parameter range. The proof-of-principle experiment based on room temperature EIT is consistent with the theoretical calculation. The response of the diode to the probe field is linear, so that it is suitable for probe fields of low intensities. The moving crystal concept also can be applied in other novel photonic devices, such as optically tunable mirrors and cavities.

We thank R. B. Liu and A. Crosse for helpful discussion. This work was supported by National Basic Research Program of China (Grants No. 2012CB921603, No. 2011CB922203, and No. 2010CB923102), National Natural Science Foundation of China (Grants No. 11174026 and No. 11274210), and CUHK Focused Investments Scheme.

*junxiang@sxu.edu.cn

[1] L. J. Aplet and J. W. Carson, Appl. Opt. **3**, 544 (1964).
[2] I. V. Shadrivov, V. A. Fedotov, D. A. Powell, Y. S. Kivshar, and N. I. Zheludev, New J. Phys. **13**, 033025 (2011).
[3] M. Scalora, J. P. Dowling, C. M. Bowden, and M. J. Bloemer, J. Appl. Phys. **76**, 2023 (1994).
[4] M. D. Tocci, M. J. Bloemer, M. Scalora, J. P. Dowling, and C. M. Bowden, Appl. Phys. Lett. **66**, 2324 (1995).
[5] S. V. Zhukovsky and A. G. Smirnov, Phys. Rev. A **83**, 023818 (2011).
[6] K. Gallo and G. Assanto, J. Opt. Soc. Am. B **16**, 267 (1999).
[7] V. V. Konotop and V. Kuzmiak, Phys. Rev. B **66**, 235208 (2002).
[8] M. S. Kang, A. Butsch, and P. S. Russell, Nat. Photonics **5**, 549 (2011).
[9] A. Kamal, J. Clarke, and M. H. Devoret, Nat. Phys. **7**, 311 (2011).
[10] L. Fan, J. Wang, L. T. Varghese, H. Shen, B. Niu, Y. Xuan, A. M. Weiner, and M. H. Qi, Science **335**, 447 (2011).
[11] Y. Shoji, T. Mizumoto, H. Yokoi, I. Hsieh, and R. M. Osgood, Appl. Phys. Lett. **92**, 071117 (2008).
[12] L. Bi, J. Hu, P. Jiang, D. H. Kim, G. F. Dionne, L. C. Kimerling, and C. A. Ross, Nat. Photonics **5**, 758 (2011).
[13] Z. F. Yu and S. H. Fan, Nat. Photonics **3**, 91 (2009).
[14] A. Alberucci and G. Assanto, Opt. Lett. **33**, 1641 (2008).
[15] F. Biancalana, J. Appl. Phys. **104**, 093113 (2008).
[16] Y. Shen, M. Bradford, and J.-T. Shen, Phys. Rev. Lett. **107**, 173902 (2011).
[17] M. D. Eisaman, A. Andre, F. Massou, M. Fleischhauer, A. S. Zibrov, and M. D. Lukin, Nature (London) **438**, 837 (2005).
[18] M. Fleischhauer, A. Imamoglu, and J. P. Marangos, Rev. Mod. Phys. **77**, 633 (2005).
[19] B. Wu, J. F. Hulbert, E. J. Lunt, K. Hurd, A. R. Hawkins, and H. Schmidt, Nat. Photonics **4**, 776 (2010).
[20] D. Hockel and O. Benson, Phys. Rev. Lett. **105**, 153605 (2010).
[21] H. Lira, Z. Yu, S. Fan, and M. Lipson, Phys. Rev. Lett. **109**, 033901 (2012).
[22] F. Biancalana, A. Amann, A. V. Uskov, and E. P. O'Reilly, Phys. Rev. E **75**, 046607 (2007).
[23] M. Artoni and G. C. La Rocca, Phys. Rev. Lett. **96**, 073905 (2006).
[24] M. D. Lukin, M. Bajcsy, and A. S. Zibrov, Nature (London) **426**, 638 (2003).
[25] M. Fleischhauer and M. D. Lukin, Phys. Rev. Lett. **84**, 5094 (2000).
[26] A. Andre and M. D. Lukin, Phys. Rev. Lett. **89**, 143602 (2002).
[27] S. Fan, R. Baets, A. Petrov, Z. Yu, J. D. Joannopuolos, W. Freude, A. Melloni, M. Popovic, M. Vanwolleghem, D. Jalas, M. Eich, M. Krausse, H. Renner, E. Brinkmeyer, and C. R. Doerr, Science **335**, 38 (2012).
[28] J. X. Zhang, H. T. Zhou, D. W. Wang, and S. Y. Zhu, Phys. Rev. A **83**, 053841 (2011).
[29] H.-T. Zhou, D.-W. Wang, D. Wang, J.-X. Zhang, and S.-Y. Zhu, Phys. Rev. A **84**, 053835 (2011).
[30] E. B. Aleksandrov and A. B. Mamyrin, Zh. Eksp. Teor. Fiz. **72**, 471 (1977).
[31] W. G. Yang, D. B. Conkey, B. Wu, D. L. Yin, A. R. Hawkins, and H. Schmidt, Nat. Photonics **1**, 331 (2007).